Applied Energy 187 (2017) 50–61

Contents lists available at ScienceDirect

Applied Energy

journal homepage: www.elsevier.com/locate/apenergy

Blackout prediction in interconnected electric energy systems considering generation re-dispatch and energy curtailment

Sadegh Kamali, Turaj Amraee *

Department of Electrical Engineering, K.N. Toosi University of Technology, Tehran, Iran

HIGHLIGHTS

- Proposing a new approach for predicting and mitigating blackout in power systems.
- Proposing an optimization model to split a power system into isolated islands.
- Developing a blackout predictor using the information gain of input impedance data.
- Splitting an unstable electric energy system with minimum energy curtailment.

ARTICLE INFO

Article history:
Received 4 July 2016
Received in revised form 21 October 2016
Accepted 13 November 2016

Keywords:
Blackout
Islanding
Prediction
Data mining
Load curtailment
Generation re-dispatch

ABSTRACT

Blackouts or cascading outages are costly events that threaten the integrity of electric energy systems around the world. Controlled splitting is executed as the last countermeasure to reduce the undesired economic and social consequences of a blackout. In this paper, a new two-stage scheme is proposed to predict the risk of a blackout in electric energy systems. In the first stage, the boundaries of electric islands are determined using a Mixed Integer Non-Linear Programming model that minimizes the cost of generation re-dispatch and load curtailment. In the second step, a data-mining technique is perfected to predict the risk of electrical separation of an electric island from the rest of the network. Each predictor is trained based on the phasor-measurement data taken at the synchronous generator terminals. Using a wide-area measurement system, the required phasor measurements are gathered and processed in the Energy Management System. Various scenarios, including the island and non-island conditions, are generated and then utilized by the decision-tree classification technique to predict the risk of a blackout. The proposed algorithm is simulated over the IEEE 39-bus test system to demonstrate its performance in online applications.

1. Introduction

1.1. Background and literature review

Energy security is defined as the reliable and uninterrupted supply of energy that is sufficient to meet the needs of the economy, and is at the same time, reasonably priced [1]. Based on this definition, four dimensions of energy security including physical, economic, social, and environmental aspects are defined. In a blackout, as a physical disruption, the electric energy production is stopped temporarily [1]. The supply disruption of an energy source causes damage, and the economic system of a country incurs costs in terms of Gross Domestic Product (GDP) loss [1,2]. The critical infrastructures are directly and interdependently impacted by major power outages. The main undesired consequences of a power outage include traffic paralysis, communication interruption, social disorder, financial and stock-market interruptions, industrial safety issues and damages, government and health-sector issues, water supply and transportation issues, manufacturing concerns, food distribution, etc. [3]. As an example, after the 2003 US and Canada blackout, 61,800 MW of power was lost for up to two days. The total impact on US workers, consumers, and taxpayers was a loss of approximately $6.4 billion directly due to the effects of electric power [4].

Because of economic reasons, electric energy systems are operated near their stable boundaries. Under heavy-load conditions, a severe contingency (i.e., a simultaneous outage of two or more important equipment), may initiate cascading outages and the power system may lose a large amount of equipment. This

* Corresponding author.
E-mail addresses: s.kamali@ee.kntu.ac.ir (S. Kamali), amraee@kntu.ac.ir (T. Amraee).

http://dx.doi.org/10.1016/j.apenergy.2016.11.040
0306-2619/

Nomenclature

CR_{ij}	correlation ratio between machines i and j
δ	rotor angle of machine
Z	impedance
ρ_i^+, ρ_i^-	cost of increasing and decreasing power generation at ith node
$\Delta P_{G_i}^-$	incremental generation re-dispatch
$\Delta P_{G_i}^+$	decremental generation re-dispatch
ΔP_{L_i}	load curtailment at *ith* load point
λ_i	cost of load curtailment at ith node
N_g	number of generation units
N_l	number of load points
N	number of nodes
N_{is}	number of electric islands
Ω^g	set of generation units
Ω^d	set of load points
Ω^l	set of transmission lines
P_{Gi}^0	initial active power generation at ith node
P_{Li}^0	initial consumption at ith node
U_{ij}	connecting check binary variable
V_i	voltage magnitude of bus i
θ	voltage angle of bus i
Y	admittance matrix
m_k	arbitrary column in Y_k
n_k	dimension of square matrix Y_k
$\|Z_1\|$	impedance sample after fault occurrence
$\|Z_2\|$	impedance sample before fault clearing
$\|Z_3\|$	impedance sample after fault clearing
$\|Z_1^w\|$	$\|Z_1\|$ for West island
$\|Z_1^s\|$	$\|Z_1\|$ for South island
$\|Z_1^N\|$	$\|Z_1\|$ for North island
$F(C_n, D_j)$	frequency of data with negative class
D_j	set of training input data at node j
$F(C_p, D_j)$	frequency of data with positive class
$E_A(D)$	entropy of attribute A over D
Q_{Gi}	reactive power generation at ith node
Q_{Li}	reactive power load at ith node
P_{ij}	the active power flow across line ij
H_i	inertia time constant of ith machine
ω_{COI}	center of Inertia speed
δ_{COI}	center of Inertia rotor angle

situation is a cascading failure, and it may expose the power system to a partial or complete blackout.

This paper focuses on the prediction and mitigation of blackouts, which are key challenges in every energy-management system. The mitigation of a blackout depends on the use of preventive or corrective measures. Preventive measures are considered in power-system expansion planning, and include installation of adequate power plants and transmission circuits. Preventive measures are long-term solutions for blackout mitigation. Different long-term strategies can be implemented to reduce the risk of blackouts, such as integration of distributed generators at load centers [5], demand side management using autonomous polygeneration [6], strategic application of microgrids [7], intelligent multiagent system theories [8], optimal design and operation of distributed energy systems [9,10] and transmission networks [11]. The roles of distributed generators and autonomous microgrids (MGs) in increasing the stability, reliability, and economy of electric energy systems have been discussed in [12–14]. Energy Management Systems (EMSs) have corrective measures for blackout mitigation. Among these measures, the last resort is the intentional splitting of an interconnected power system into stable isolated electric islands. During a cascading failure or blackout, a group of generating units or power plants tends to be electrically separated from the rest of the network. This condition is called uncontrolled islanding and it may cause a blackout due to which many load centers and generation units will be lost. Controlled splitting or islanding is the last corrective measure to avert this cascading failure and reduce the extent of a blackout. Controlled islanding refers to splitting an interconnected power system into a number of stable independent islands at suitable times and proper locations [15]. To have an efficient controlled islanding, the blackout must be predicted before experiencing a critical transition. In each controlled islanding strategy, two different issues: "where to split?" and "when to split?" must be considered. Many approaches have been presented to address the "where to split" issue of a large power system following a widespread contingency. For the "where to split" issue, the proper points of splitting are found using the coherency coefficients of synchronous generators or through combinations of optimization techniques and graph-theory methods [16–21]. For the "when to split" issue, the blackout is predicted using suitable measurements [22–24]. In [22], the time of controlled islanding (i.e., "when to island") is predicted by a decision tree (DT) using phasor measurements. In [23], a DT-assisted scheme has been presented to determine the timing of controlled islanding in real time using phasor measurements. In [24], the security boundaries are determined by the rules of DTs that are developed from the generated knowledge bases. The previous proposed schemes for the "where to split" aspect act based on the graph theory, without considering the cost of generation re-dispatch or load curtailment. Furthermore, the simultaneous modeling of "where to split" and "when to split" aspects have not been considered in literature. The intention of this paper is to consider both aspects sequentially. The former issue is considered using a Mixed Integer Non-Linear Programming (MINLP) model and the latter issue is implemented using the DT technique. The DT technique predicts the blackout using the impedance measurements at generator terminals.

1.2. Contributions

This paper presents a new two-stage algorithm to predict the risk of a blackout in interconnected power systems. In the first stage, the boundaries of electric islands (i.e., the splitting points) are determined using an MINLP formulation to reduce the cost of generation re-dispatch and load curtailment. The proposed MINLP formulation is an efficient alternative for the graph-based methods. In the second stage, a DT classifier is trained for blackout prediction in each electric island. The proposed classifier predicts the blackouts using the information gained from the input phasor measurements. In other words, the proposed scheme acts as a wide-area blackout predictor that predicts the electric separation of each island from the rest of the network.

1.3. Paper organization

This paper is organized as follows: In Section 2, a simple cascading outage (i.e., blackout) is simulated for a typical two-area test grid. In Section 3, the formulation of the proposed MINLP-based splitting strategy and the fundamentals of the DT classifier are

described. In Section 4, simulation results are discussed. Finally, Section 5 presents the conclusions of this paper.

2. Uncontrolled islanding and blackout

Cascading failure refers to a sequence of dependent outages, which may cause a large blackout in integrated power systems [15]. A key to blackout mitigation is to predict the system response and identify correct remedial actions. Different remedial actions or system protection schemes (SPSs) can be used for blackout mitigation [25]. Loss of synchronism or out-of-step tripping, and line outages are the initial symptoms of this costly event. Actually, the blackout happens when a severe fault in the power system causes one or more groups of coherent generators to be out-of-step. These events will continue until the blackout has spread to a large part of the network. For better clarification of the blackout phenomenon, a two-area test system (as shown in Fig. 1) is used [26].

The system is exposed to a delayed three-phase short-circuit (SC) fault at t = 1 s at the middle of the transmission line 7–8. This SC fault is cleared at t = 1.3 s by line tripping. As shown in Fig. 2, following this initial contingency, the generators 1 and 2 (i.e. G1 and G2) remain coherent (i.e., having consistent rotor-angle trajectories) and are electrically separated from the rest of the network (i.e., become out-of-step) at t = 2.6 s. As shown in this figure, a blackout in this situation is inevitable because of the electrical separation of the coherent groups. Controlled islanding is the final remedial action to prevent the blackout in this situation. However, to design an efficient controlled-splitting strategy, the time of the blackout must be predicted. Blackouts can be predicted using event-based or response-based strategies. In an event-based strategy, power-system islanding is detected using the out-of-step monitoring of synchronous generators. In the response-based strategy, the measurements of the system response are processed by analytic or data-mining techniques for blackout prediction. Furthermore, the utilized algorithm must predict the unplanned islanding before the activation of out-of-step relays. The result of this prediction is used to trigger the controlled islanding strategy (i.e., the "when to island" issue is determined).

3. Proposed prediction strategy

In this section, the proposed strategy for islanding prediction is presented. The overall structure of the prediction method is shown in Fig. 3. As shown in this figure, the proposed method has two distinct parts: (a) offline construction of the blackout-prediction module, and (b) online application. Details of the proposed approach are described in steps 1–7.

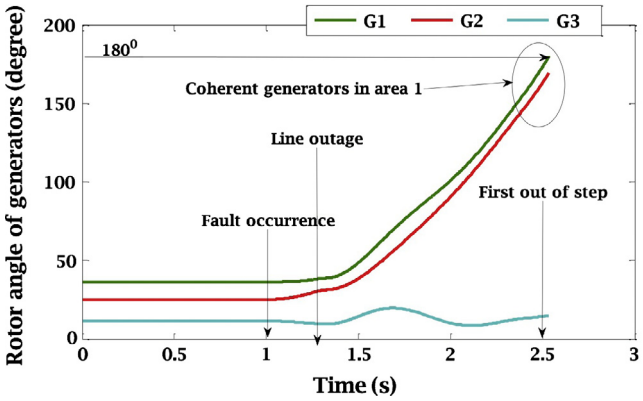

Fig. 2. Rotor-angle trajectories of generators following an SC fault.

3.1. Step 1 and step 2

Based on the power-system topology and operational conditions, the synchronous generators are classified into several electric coherent groups. In the first step, the coherent generators are determined using the slow coherency technique. To determine the coherent generators, the correlation coefficients between the rotor angles of all pairs of generators are calculated. The correlation ratio between two vectors of rotor angles is utilized as the coherency criteria. The correlation coefficient between two machines is calculated as follows [27]:

$$CR_{ij} = \frac{n\sum_{t=1}^{n}[\delta_i(t)\delta_j(t)] - \sum_{t=1}^{n}[\delta_i(t)] \times \sum_{t=1}^{n}[\delta_j(t)]}{\sqrt{\left[n\sum_{t=1}^{n}(\delta_i(t))^2 - \left(\sum_{t=1}^{n}\delta_i(t)\right)^2\right] \times \left[n\sum_{t=1}^{n}(\delta_j(t))^2 - \left(\sum_{t=1}^{n}\delta_j(t)\right)^2\right]}} \quad (1)$$

The second important step is to recognize the boundaries of islands and to minimize the real power imbalance in each island when coherent generators are placed in the same group. This step may support the stability of each island. The boundaries of electric islands are determined using an MINLP formulation. The objective function of the MINLP-based splitting strategy minimizes the cost of generation re-dispatch and load curtailment as follows:

$$\min \quad Cost = \sum_{i=1}^{N_g}\rho_i^+ .\Delta P_{G_i}^+ + \sum_{i=1}^{N_g}\rho_i^- .\Delta P_{G_i}^- + \sum_{i=1}^{N_l}\lambda_i .\Delta P_{L_i} \quad (2)$$

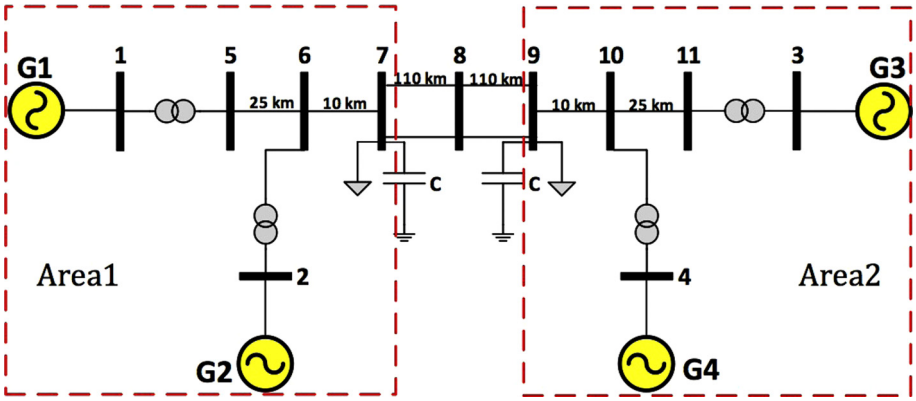

Fig. 1. Single-line diagram of two-area test system.

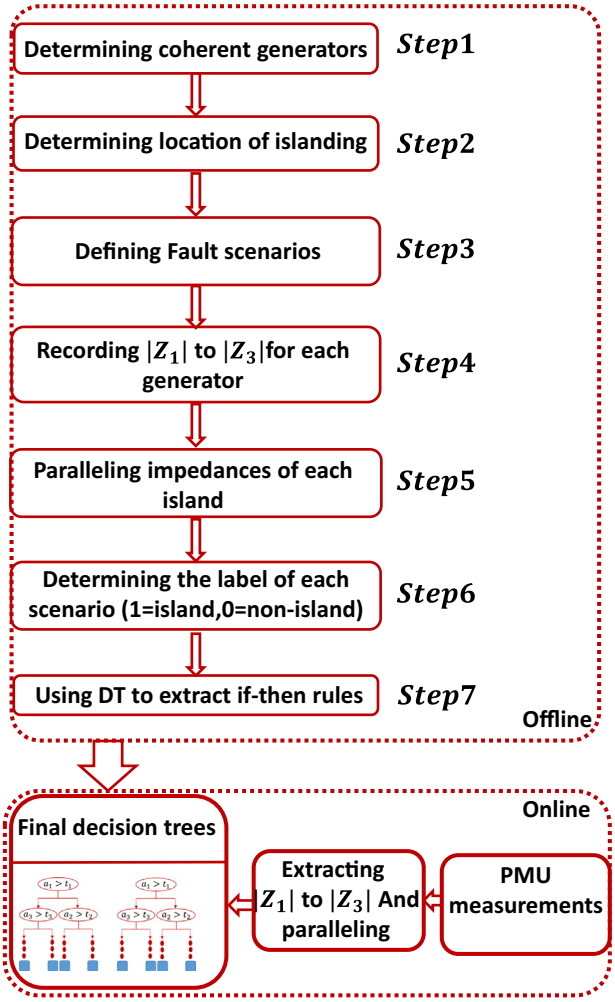

Fig. 3. Overall structure of islanding prediction algorithm.

It is noted that the cost of load curtailment is much more than the cost of generation re-dispatch. This issue will be considered in the simulation results. The set of constraints in the MINLP-based islanding strategy are defined as follows.

3.1.1. Power-balance constraint

The active and reactive power-balance constraints at each node of each island are expressed via the AC load-flow equations as follows:

$$[P_{Gi}^{0}+\Delta P_{Gi}^{+}-\Delta P_{Gi}^{-}-(P_{Li}^{0}-\Delta P_{Li})]U_{ij}=V_i\sum_{n=1}^{N}V_kY_{in}\cos(\delta_i-\delta_k-\theta_{in}) \tag{3}$$

$$[Q_{Gi}-Q_{Li}]U_{ij}=V_i\sum_{n=1}^{N}V_kY_{in}\sin(\delta_i-\delta_n-\theta_{in})$$
$$i=1,\ldots,N \text{ and } j=1,\ldots,N_{is}$$

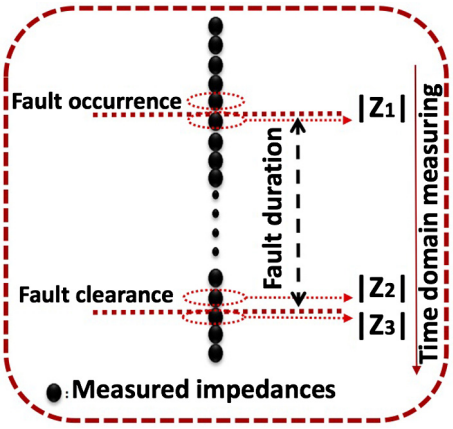

Fig. 4. Required impedances as the input samples for DT.

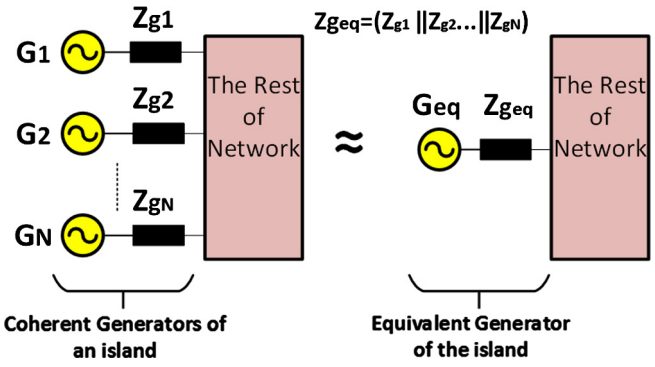

Fig. 5. Equivalent of coherent generators in islanding scheme.

3.1.2. Operational constraints

The limits of the transmission lines, the upper and lower limits of generation re-dispatch, and the upper limit of load curtailment are expressed as follows:

$$S_{ij}\left(=\sqrt{P_{ij}^{2}+Q_{ij}^{2}}\right)\leqslant S_{ij}^{max}\quad \forall ij\in\Omega^{l} \tag{5}$$

$$-S_{ij}\leqslant S_{ij}^{max}\quad \forall ij\in\Omega^{l} \tag{6}$$

$$0\leqslant\Delta P_{Gi}^{+}\leqslant\Delta P_{Gi}^{+max}\quad \forall i\in\Omega^{g} \tag{7}$$

$$0\leqslant\Delta P_{Gi}^{-}\leqslant\Delta P_{Gi}^{-max}\quad \forall i\in\Omega^{g} \tag{8}$$

$$0\leqslant\Delta P_{L_i}\leqslant\Delta P_{L_i}^{max}\quad \forall i\in\Omega^{g} \tag{9}$$

$$Q_{Gi}^{min}\leqslant Q_{Gi}\leqslant Q_{Gi}^{max}\quad \forall i\in\Omega^{g} \tag{10}$$

$$V_i^{min}\leqslant V_i\leqslant V_i^{max}\quad \forall i\in\Omega^{d} \tag{11}$$

Table 1
List of input scenarios.

Fault type	3-Phase short circuit followed by a single line outage	3-Phase short circuit followed by double line outages
Fault occurring time	at t = 0.1 s	First fault at t = 0.10 s and the second fault at t = 0.11 s
Fault clearing time	Changing from 120 ms to 400 ms in steps of 20 ms	First fault: cl1 = 120 ms to 500 ms Second fault: cl2 = cl1 + 50 ms
Total number of scenarios	544	512

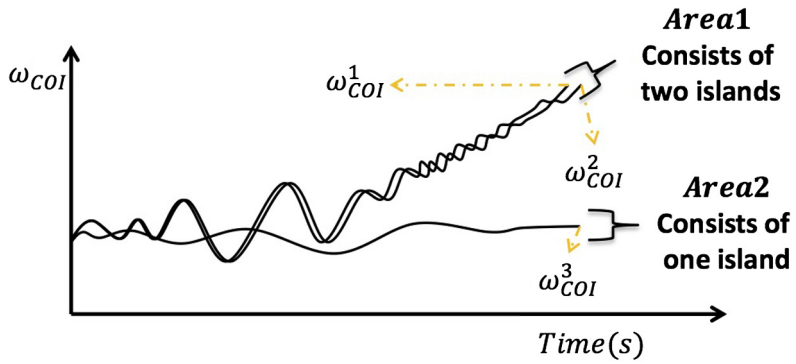

Fig. 6. Classification rule for the test grid with three islands.

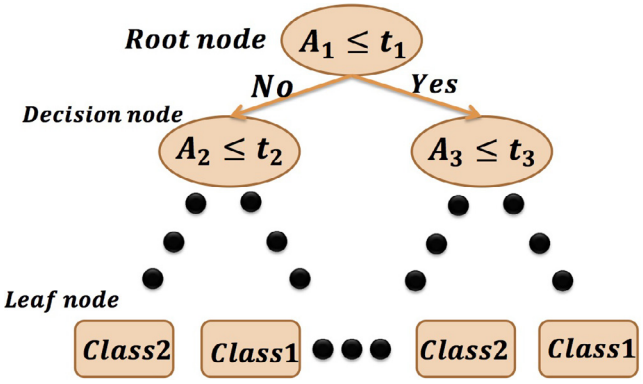

Fig. 7. Typical biclass DT.

3.1.3. Grouping constraint

Based on this constraint, each load point belongs to only one island.

$$\sum_{j=1}^{N_{is}} U_{ij} = 1 \quad for \quad i = 1, 2, \ldots, N_l \tag{12}$$

If the ***ith*** load bus belongs to the ***jth*** island, the binary variable U_{ij} will be equal to 1 (i.e., $U_{ij} = 1$).

Table 2
Coherent generators in IEEE 39-bus test system.

Island	Coherent generators
North Island	30, 37, 38
West Island	31, 32, 39
South Island	33, 34, 35, 36

Table 3
Generation re-dispatch and load curtailment of all nodes.

Bus no	Generation re-dispatch and load curtailment		
	ΔP_G^+ (MW)	ΔP_G^- (MW)	ΔP_D (MW)
30	0	146.5	0
31	214.32	0	0
33	0	67.86	0
Other nodes	0	0	0
Total change (MW)	214.32	214.36	0
Total cost ($/h)	32148.315	12,068	0

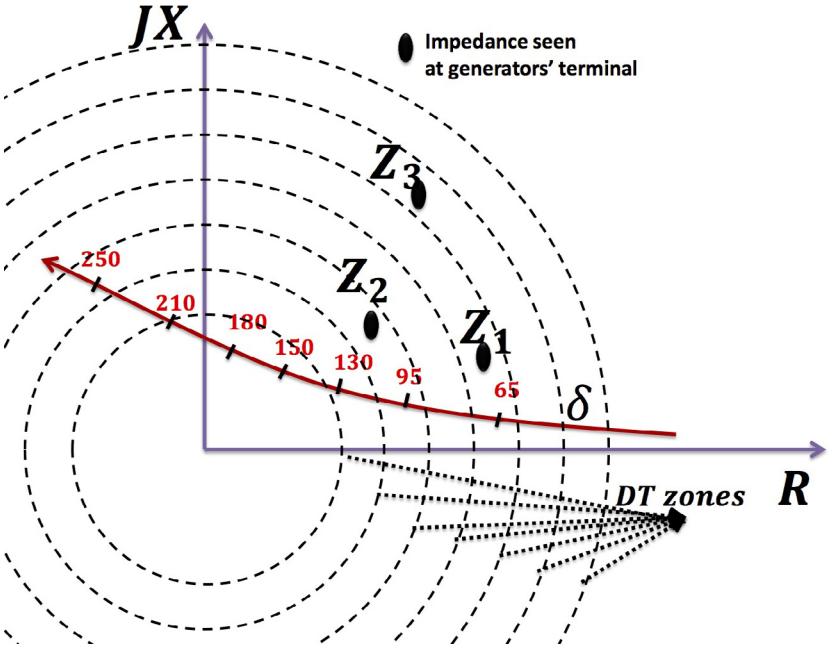

Fig. 8. Conceptual zones learned by decision tree.

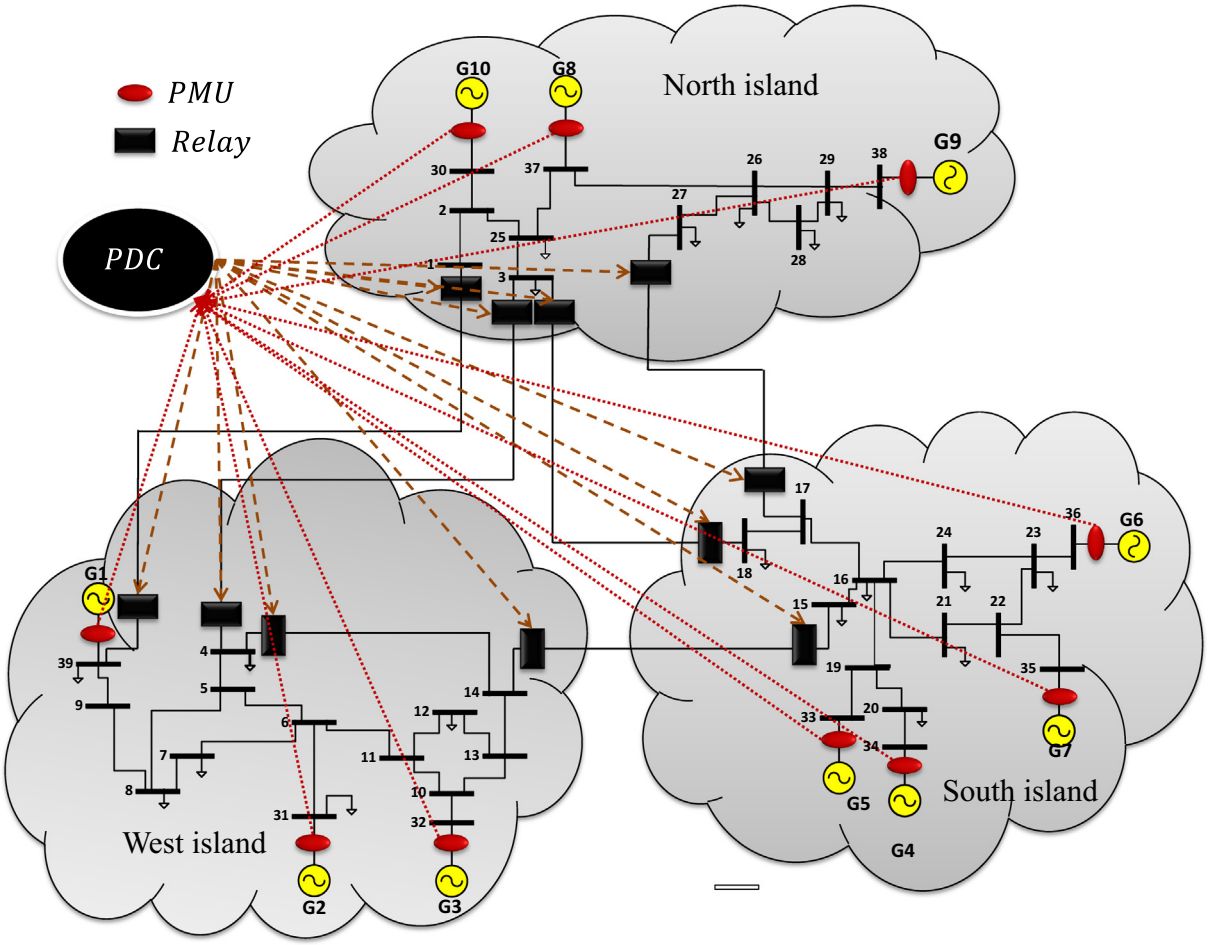

Fig. 9. Obtained boundaries (i.e., islands) for IEEE 39-bus network using MINLP formulation.

3.1.4. Connectivity constraint

Based on this constraint, there is a path between every pair of nodes in each island. The graph of each island is connected if every node in the graph (e.g., node m_k) is reachable from every other node in that graph. The connectivity of each island is formulated as a linear constraint as follows:

$$\boldsymbol{Y}_{\boldsymbol{k}}^{-1}(\boldsymbol{i},\boldsymbol{m}_{\boldsymbol{k}})\neq\boldsymbol{0} \quad \forall \boldsymbol{i}\in\boldsymbol{n}_{\boldsymbol{k}} \tag{13}$$

3.2. Step 3

Nowadays, practical out-of-step relays detect the loss of synchronism by monitoring the rate of change of equivalent impedance observed at the generator's terminal. In out-of-step relays, the way-in and way-out blinders measure the time variation of impedance (i.e. $\Delta Z/\Delta t$) to distinguish between out-of-step and other conditions. Therefore, in this paper, the equivalent impedances observed at the generators' terminals are utilized to predict the blackout. The proposed scheme acts as a wide-area out-of-step predictor. However, unlike the local out-of-step relays, the proposed wide-area out-of-step predictor is used to detect the out-of-step conditions between electric islands. Many input scenarios, including island and non-island conditions, are simulated and are used as the input data for the DT construction. All credible N − 1 (i.e., outage of a single equipment) and N − 2 (i.e., simultaneous outages of two equipment) contingencies are considered. Details of the input scenarios are given in Table 1.

3.3. Step 4

The magnitudes of equivalent impedances seen at the generators' terminals at specified instants are used as the input features. Three different samples of the equivalent impedances at fault-occurring and clearing times (i.e., $|Z_1|$ to $|Z_3|$ as shown in Fig. 4) are used as DT attributes (i.e., input features for DT training). These impedances are expressed as per-unit (i.e. pu) values. The out-of-step tripping in power systems is an important symptom of an imminent blackout. Based on the slow coherency method, the set of electric islands are determined. For each electric island, a specific DT is trained. Each DT uses all measured impedances from all generators. The DT algorithm determines the critical zones or thresholds of $|Z_1|$ to $|Z_3|$. For each input scenario, these samples are recorded and are used as inputs for the next step.

3.4. Step 5

In this step, the input features of the training samples are defined based on the coherency approach. The coherent generators can be approximated as parallel generators by neglecting the bus-voltage angle differences [28]. The main advantage of coherency-based islanding is that the resultant grouping of generators does not depend significantly on the initial conditions, size of disturbance, or generator-model detail [16]. As shown in Fig. 5, to reduce the number of decision variables, the measured impedances of the coherent generators in each island are paralleled, and the DT is constructed offline. Therefore, the online action of the proposed

Table 4
The comparison between the proposed MINLP method and method proposed in [32].

Utilized method	Number of splitting lines	Number of Islands	Total power imbalance (MW)
Proposed method	5 (1–39, 3–4, 3–18, 27–17, 14–15)	3	428.68
Method proposed in [32]	8 (1–2, 4–5, 12–13, 13–10, 15–16, 17–18, 25–26, 17–16)	4	933

scheme will be fast and the computational burden of the method is reduced significantly. For a given input scenario (i.e., simulation event), three samples of the equivalent impedance are recorded for each generator bus. This results in a DT with a simple structure.

3.5. Step 6

In this step, the output features of the training samples (i.e., the target class of input samples) are defined. The target class of each input sample is defined as **Island** or **Non-Island**. For each island, to determine the final state of any input scenario, the rotor angle and speed at the center of inertia (COI) reference are used. The COI speed and angle are calculated for each island as follows [26]:

$$\delta_{COI} = \frac{\sum_{i=1}^{n} H_i \delta_i}{\sum_{i=1}^{n} H_i} \tag{14}$$

$$\omega_{COI} = \frac{d\delta_{COI}}{dt} \tag{15}$$

The target class of each island is assigned using the following classification rule. For a multi-island network, when one island is about to be electrically separated from the rest of network, its target class becomes Island while the target class of the rest of the network is Non-Island. This rule has been illustrated in Fig. 6 for the IEEE 39-bus test system with three coherent groups or islands. As shown in Fig. 6, the target class of Area2 is Island and the target class of Area1 is Non-Island.

3.6. Step 7

A classification problem is a prediction task in which the classifier is constructed based on a set of input–output samples, considering the efficient attributes of a system. Prediction is done easily by DT and the threshold of the attribute with the highest information gain is then extracted for classification. The typical structure of a DT is illustrated in Fig. 7.

The prediction rule is extracted using a series of if–then rules from the root node toward the leaf node. Each leaf node (as the final node) contains the target class that is the end point of the prediction procedure. Different algorithms can be used for the DT construction. In this paper, C4.5 is utilized to train DTs based on the concept of information entropy [29]. Entropy is defined as follows [29]:

$$E(D_j) = -\frac{F(C_n, D_j)}{|D_j|} \times \mathrm{Ln}\left(\frac{F(C_n, D_j)}{|D_j|}\right) - \frac{F(C_p, D_j)}{|D_j|} \times \mathrm{Ln}\left(\frac{F(C_p, D_j)}{|D_j|}\right) \tag{16}$$

where $|D_j|$ is the number of samples in D_j. For a biclass problem, it is assumed that each node has two child nodes, including the Yes and No outgoing branches. To find the most important attribute at each node, the entropy of all attributes over the input data must be computed as follows:

$$E_A(j) = -\frac{|D_{j,A}^{NO}|}{|D_j|} \times E(D_{j,A}^{NO}) - \frac{|D_{j,A}^{Yes}|}{|D_j|} \times E(D_{j,A}^{Yes}) \tag{17}$$

where $|D_{j,A}^{NO}|$ is the number of samples located in branch NO considering the attribute A, $|D_{j,A}^{Yes}|$ is the number of samples located at node j in branch YES considering the attribute A. After calculating the entropy of each attribute at a given node, the gain of classification using the attribute A is computed as follows:

$$G_A(j) = E(D_j) - E_A(j) \tag{18}$$

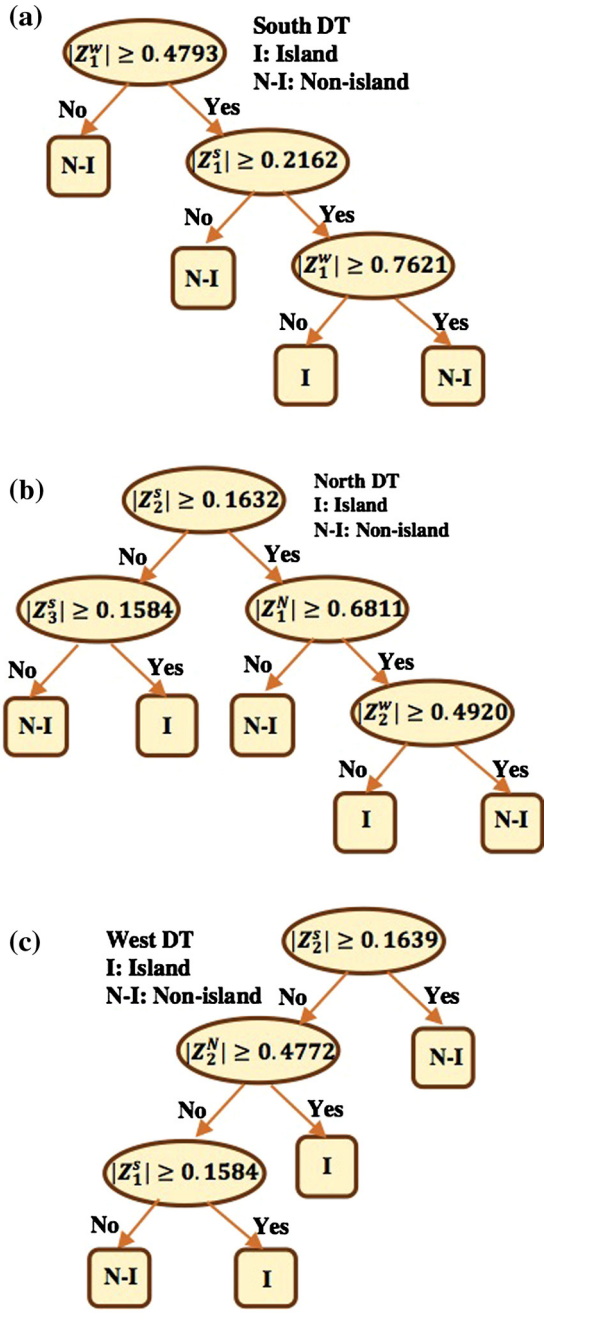

Fig. 10. Final constructed DTs obtained for each island (a) South Island, (b) North Island, (c) West Island.

In this paper, the gain ratio is used as the performance criteria. The gain ratio is introduced as follows:

$$GR_A(j) = \frac{G_A(j)}{SE_A(j)} \tag{19}$$

where

$$SE_A(j) = -\frac{|D_{j,A}^{NO}|}{|D_j|} \times Ln\left(\frac{|D_{j,A}^{NO}|}{|D_j|}\right) - \frac{|D_{j,A}^{Yes}|}{|D_j|} \times \mathrm{Ln}\left(\frac{|D_{j,A}^{Yes}|}{|D_j|}\right) \tag{20}$$

At each decision node, the attribute with the highest gain ratio is selected as the decision criterion at that node. This process must be repeated for all decision nodes.

The final step in the offline mode is the creation of the DT based on the input–output data sampled from predefined simulation scenarios. After assigning the labels for each input scenario and sampling the required impedances, these data are used to train and test the DT-based classifier. For the IEEE 39-bus test system, three different islands are assumed. Therefore, three DTs are constructed. Each pair of input–output samples is defined as follows:

$$(Input{:}Output)_i = \left(|Z_1^1|_i|Z_2^1|_i|Z_3^1|_i, \ldots, |Z_1^{N_{is}}|_i|Z_2^{N_{is}}|_i|Z_3^{N_{is}}|_i{:}Ibit_i\right)$$
$$i = 1, \ldots, N_s$$

As shown in Fig. 8, the DT classifier learns the thresholds of these impedances as conceptual operating zones in the R–X plane.

4. Simulation results

In this section, the proposed algorithm is applied to the IEEE 39-bus 10-machine test system. The static and dynamic data of this case study can be found in [30]. Transient stability simulations are done using DIgSILENT software on a PC with Intel Corei5 3.2 GHz CPU and 4 GB RAM. All synchronous machines were equipped with IEEE DC1 excitation systems and a standard governor. The simulation results are presented in four parts. In the first part, the details of the input scenarios are presented. In the second part, the coherent generators of the test system are determined. The final extracted DTs for blackout prediction are presented in the third part, and the performance of the proposed algorithm is investigated for an unseen contingency in the fourth part.

4.1. Scenario construction

A comprehensive list of input scenarios was created for the DT training. Different factors such as duration and location of SC faults were considered while creating the input scenarios. In this study, 1056 input scenarios were defined based on Table 1. For each input scenario, a 15-s transient stability simulation was carried out. As shown in Table 1, each three-phase SC is followed by a single or double-line outage. The fault duration was changed from 100 ms to 400 ms in steps of 20 ms. In case of a three-phase SC with double-line outage, it was assumed that two consequent SC faults occurred at t = 0.1 s and t = 0.12 s; they were cleared after t = cl_1 s and t = cl_2 s, respectively.

Based on the pairwise correlation coefficients, the coherent generators were determined as presented in Table 2. For each coherent group of generators, an electric island was formed. Therefore, three different islands named W (West), S (South), and N (North) were defined. The boundaries of these islands were determined using the proposed MINLP formulation, which was solved using the CPLEX algorithm. The costs of generation re-dispatch and load curtailment were assumed as $\rho_i^+ = 150\frac{\$}{MWh}, \rho_i^- = 50\frac{\$}{MWh}$ and $\lambda_i = 1500\frac{\$}{MWh}$ [31]. The cost of generation decrement is an opportunity cost. In this paper, the cost of energy curtailment is

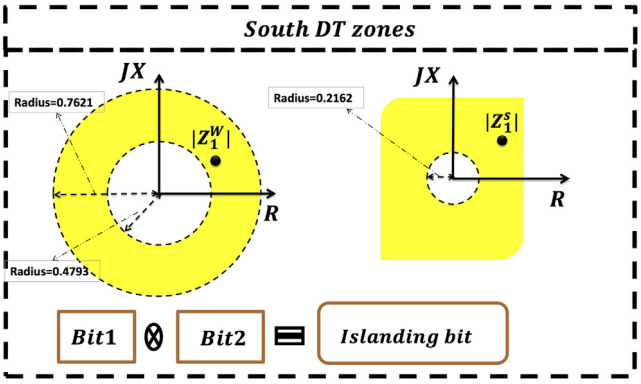

Fig. 11a. Conceptual blinders or zones obtained for South Island.

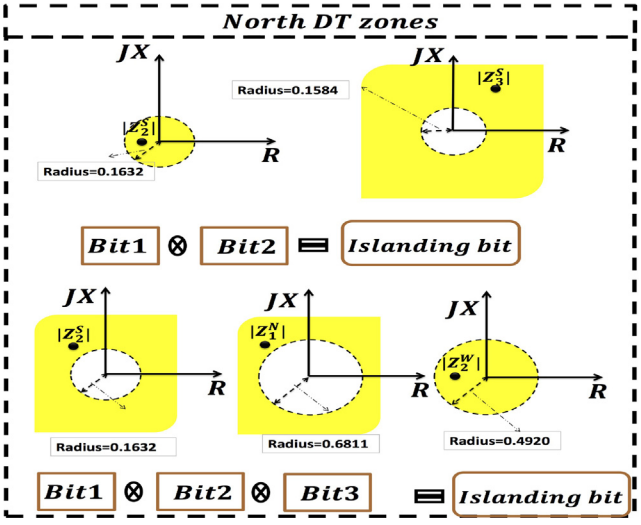

Fig. 11b. Conceptual blinders or zones obtained for North Island.

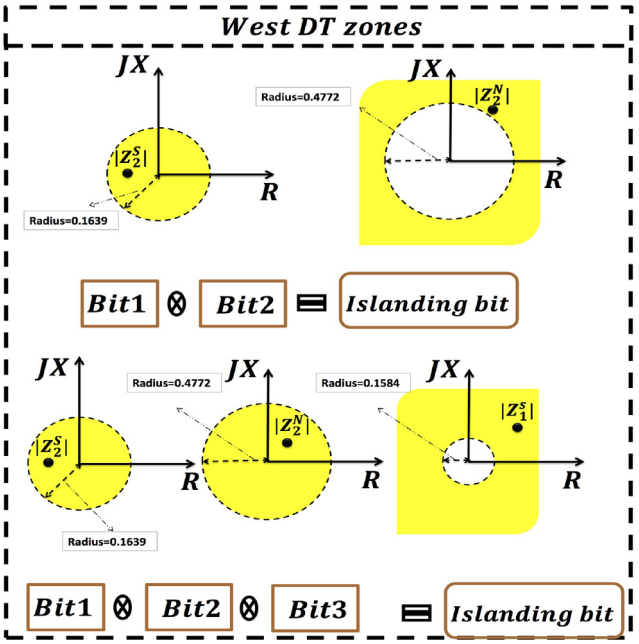

Fig. 11c. Conceptual blinders or zones obtained for West Island.

Table 5
The comparison between the proposed predictor and method proposed in [22].

Actual class	Proposed method		Rotor angle method [22]	
	Classified as non-Island	Classified as Island	Classified as non-Island	Classified as Island
Island (216)	12	204	63	153
Non-island (840)	831	9	745	95
Total misclassified	21 (12 + 9)		158 (63 + 95)	
Accuracy of classification (%)	98.011%		85.038%	

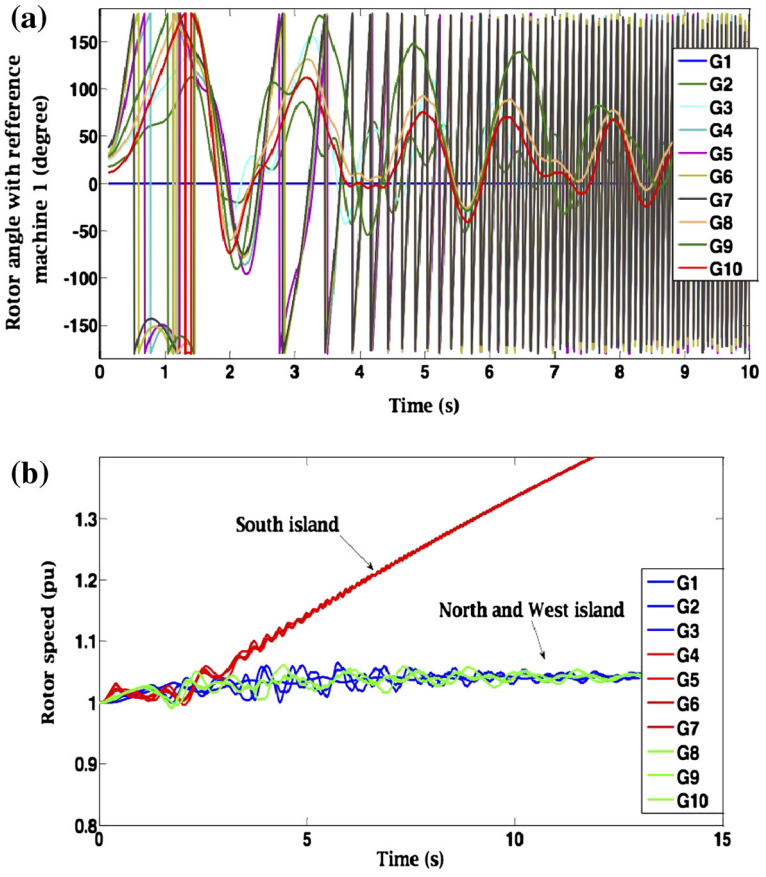

Fig. 12. (a) Variation of rotor angles w.r.t generator 1 following an SC fault at bus 16. (b) Variation of rotor speeds w.r.t generator 1 following an SC fault at bus 16.

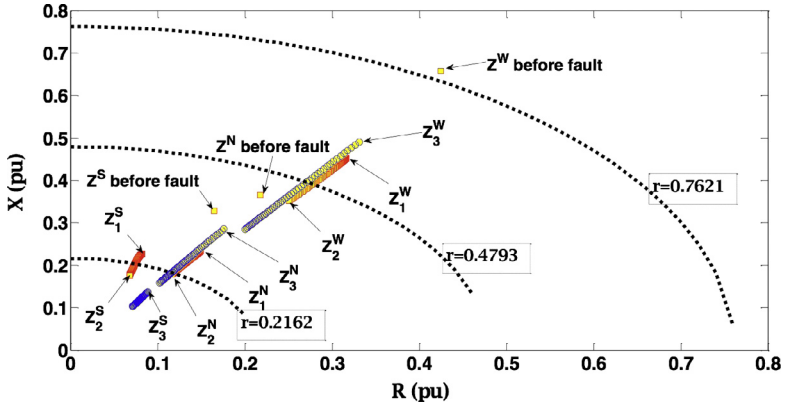

Fig. 13. Impedance variation in R–X plane following an SC fault at bus 16.

assumed 10 times the cost of generation increment. The obtained boundary for each island and the required generation re-dispatch and load curtailment are given in Table 3 and Fig. 9. Based on Table 3, due to the high penalties for load curtailment, the splitting strategy was executed using generation re-dispatch. In other words, the interconnected power system was divided into three

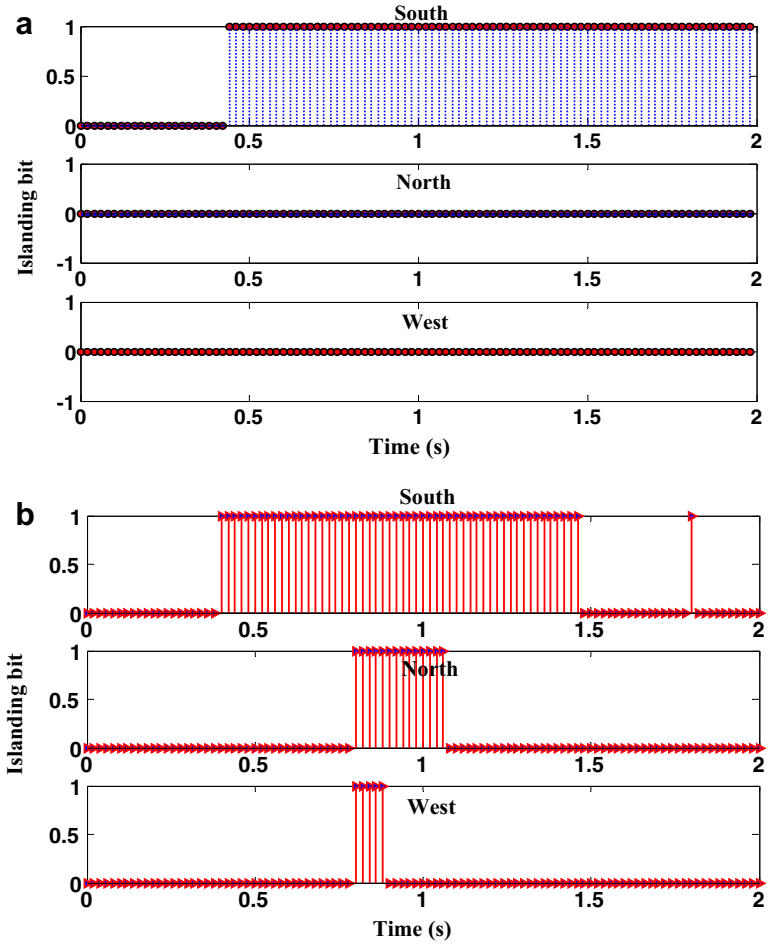

Fig. 14. (a) DT prediction following the SC fault at bus 16 using impedance data and (b) DT prediction following the SC fault at bus 16 using rotor-angle data.

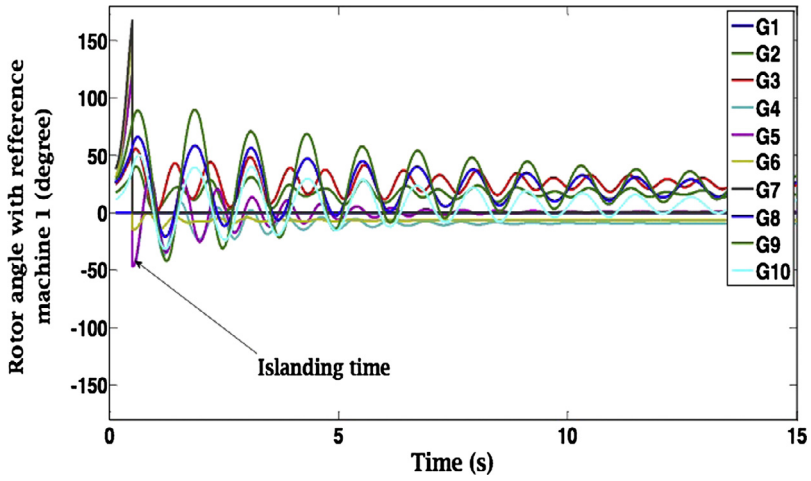

Fig. 15. Trajectories of rotor angles w.r.t generator 1 when the South Island is separated from the rest of the network at t = 0.54 s.

different islands, with 214.32 MW and 214.36 MW generation re-dispatch in increasing and decreasing directions, respectively (i.e. without any load curtailment). It was noted that, in case of a black-out (i.e., without executing the proposed scheme), a total load of 6254.2 MW (i.e., total base-case load) was be lost. In other words, without executing the proposed method a complete power outage is occurred and the base-case load of the network (i.e. 6254.2 MW) is lost. The cost of this load curtailment was about 9,381,300 $/h (i.e., 6254.2 MW $*$ 1500 $/MWh). A detailed comparison between the proposed MINLP algorithm and the proposed method in [32], is given in Table 4. According to Table 4, the number of splitting lines and the total power imbalance are decreased significantly using the proposed MINLP method. The required measurements were provided by Phasor Measurement Units (PMUs) at the gener-

ator terminals. These data were then transmitted to a Phasor Data Concentrator or EMS to decide the execution of the islanding strategy. The splitting lines were equipped with relays to send the tripping signals for the circuit breakers.

4.2. Final constructed DTs

After generating the input samples, the DTs were constructed and were used to find the critical thresholds of the attributes (i.e., $|Z_1|$ to $|Z_3|$). In practice, based on Fig. 9, the required impedances were measured by PMUs. The DTs predicted the final states of islanding before experiencing a critical transition. It was noted that each electric island had its own DT to make an independent decision (i.e., each DT predicted the final state of its island). Figs. 10and 11 show the final constructed DTs and the conceptual operating zones of each DT. It can be seen that $|Z_1$ |and $|Z_2|$ (i.e., impedances measured right after the fault occurrence and before fault clearance) have more information gain for blackout prediction. In addition, the obtained out-of-step zones by each DT are depicted in Fig. 11. For example, Fig. 11a shows that if the $|Z_1^w|$ following a disturbance is lesser than 0.7621 pu and greater than 0.4793 pu and $|Z_1^s|$ is greater than 0.2162 pu, the related target class will be Island (i.e., $I_{Bit} = 1$). Therefore, the South Island must be separated from the rest of the network at predefined splitting points. According to Table 5, in this prediction, 216 scenarios out of the 1056 input scenarios had an Island label in which 21 scenarios were misclassified by the constructed DTs. In other words, the accuracy of classification was 98.01%. The results of prediction using the rotor angle trajectory [22], are given in last column of Table 5.

4.3. Performance of the proposed algorithm

In this section, the performance of the proposed scheme is investigated following an SC fault (i.e., an unseen scenario) that was applied at 0.1 s in bus 16 and cleared after 300 ms. For this purpose, two kinds of DTs were constructed with two different input features (i.e., rotor-angle samples and proposed impedance samples). Fig. 12a shows the rotor angle of each generator after the SC fault. As shown in this figure, seven generators became unstable in less than 1.5 s. Moreover, Fig. 12b shows that, the speed trajectories of coherent generators in South Island deviate from the other generators. Therefore, if the controlled islanding strategy is not executed, the network will experience a blackout after about 2.5 s. Fig. 13 shows the impedance variations in this scenario. Fig. 14a shows the DT output (i.e., decision) following this disturbance. As shown in this figure, after 0.42 s, the DTs predict the final state of their related islands (i.e., North Island = 1, South Island = 0, West Island = 0). In addition, Fig. 14b shows the DT prediction outputs in which the rotor angles of the generators are used as the DT inputs. As shown in this figure, the outputs of the DTs trained by the rotor-angle samples provide undesired predictions for the islanding status. Fig. 15 shows the rotor angles of the generators after the separation of the South Island from the rest of the grid after 0.52 s (i.e., including 0.1 s for inherent delays). As shown in this figure, all generators have stable rotor angles.

5. Conclusion

In this paper, a two-stage scheme was proposed to predict blackouts. The proposed scheme received the impedance measurements from the generator terminals through PMUs and then sought to extract decision rules to distinguish island conditions from other non-island conditions. While the conventional out-of-step relays detected the electrical separation of one synchronous machine from the rest of the network, the proposed method acted as a wide-area out-of-step predictor to detect the electrical separation of one region with respect to the rest of the network. The boundaries of electric islands were determined using an MINLP formulation. The output of the prediction was used to trigger the controlled-splitting strategy before the occurrence of a blackout. The accuracy of the DT classifier verified the performance of the proposed impedance-based scheme.

References

[1] Jun E, Kim W, Chang SH. The analysis of security cost for different energy sources. Appl Energy 2009;86(10):1894–901.
[2] Pantoja Andrés, Quijano Nicanor. A population dynamics approach for the dispatch of distributed generators. Ind Electron, IEEE Trans 2011;58 (10):4559–67.
[3] Force UC. Final report on the august 14th blackout in the United States and Canada. Department of Energy and National Resources Canada; 2004.
[4] Bo Z, Shaojie O, Jianhua Z, Hui S, Geng W, Ming Z. An analysis of previous blackouts in the world: lessons for China' s power industry. Renew Sustain Energy Rev 2015;42:1151–63.
[5] Manfren M, Caputo P, Costa G. Paradigm shift in urban energy systems through distributed generation: methods and models. Appl Energy 2011;88 (4):1032–48.
[6] Kyriakarakos G, Piromalis DD, Dounis AI, Arvanitis KG, Papadakis G. Intelligent demand side energy management system for autonomous polygeneration microgrids. Appl Energy 2013;103:39–51.
[7] Hatziargyriou N, Asano H, Iravani R, Marnay C. Microgrids. IEEE Power Energ Mag 2007;5(4):78–94.
[8] Karavas Christos-Spyridon, Kyriakarakos George, Arvanitis Konstantinos G, Papadakis George. A multi-agent decentralized energy management system based on distributed intelligence for the design and control of autonomous polygeneration microgrids. Energy Convers Manage 2015;103:166–79.
[9] Morvaj Boran, Evins Ralph, Carmeliet Jan. Optimization framework for distributed energy systems with integrated electrical grid constraints. Appl Energy 2016;171:296–313.
[10] Falke Tobias, Krengel Stefan, Meinerzhagen Ann-Kathrin, Schnettler Armin. Multi-objective optimization and simulation model for the design of distributed energy systems. Appl Energy 2016.
[11] Guerra Omar J, Tejada Diego A, Reklaitis Gintaras V. An optimization framework for the integrated planning of generation and transmission expansion in interconnected power systems. Appl Energy 2016;170:1–21.
[12] Kanchev Hristiyan, Lu Di, Colas Frederic, Lazarov Vladimir, Francois Bruno. Energy management and operational planning of a microgrid with a PV-based active generator for smart grid applications. Ind Electron, IEEE Trans 2011;58 (10):4583–92.
[13] Lidula NWA, Rajapakse AD. Microgrids research: a review of experimental microgrids and test systems. Renew Sustain Energy Rev 2011;15(1):186–202.
[14] Detroja Ketan P. Optimal autonomous microgrid operation: a holistic view. Appl Energy 2016;173:320–30.
[15] Adibi MM, Kafka RJ, Maram S, Mili LM. On power system controlled separation. Power Syst, IEEE Trans 2006;21(4):1894–902.
[16] Yang B, Vittal V, Heydt GT. Slow-coherency-based controlled islanding &# 8212; a demonstration of the approach on the August 14, 2003 blackout scenario. Power Syst, IEEE Trans 2006;21(4):1840–7.
[17] Xu G, Vittal V, Meklin A, Thalman JE. Controlled islanding demonstrations on the WECC system. Power Syst, IEEE Trans 2011;26(1):334–43.
[18] Trodden PA, Bukhsh WA, Grothey A, McKinnon KIM. MILP formulation for controlled islanding of power networks. Int J Electr Power Energy Syst 2013;45 (1):501–8.
[19] Sun K, Zheng DZ, Lu Q. Splitting strategies for islanding operation of large-scale power systems using OBDD-based methods. Power Syst, IEEE Trans 2003;18 (2):912–23.
[20] Sun K, Zheng DZ, Lu Q. A simulation study of OBDD-based proper splitting strategies for power systems under consideration of transient stability. Power Syst, IEEE Trans 2005;20(1):389–99.
[21] Zhao Q, Sun K, Zheng DZ, Ma J, Lu Q. A study of system splitting strategies for island operation of power system: a two-phase method based on OBDDs. Power Syst, IEEE Trans 2003;18(4):1556–65.
[22] Senroy N, Heydt GT, Vittal V. Decision tree assisted controlled islanding. Power Syst, IEEE Trans 2006;21(4):1790–7.
[23] Diao R, Vittal V, Sun K, Kolluri S, Mandal S, Galvan F. Decision tree assisted controlled islanding for preventing cascading events. In: Power systems conference and exposition, 2009. PSCE'09. IEEE/PES. IEEE; 2009. p. 1–8.
[24] Genc I, Diao R, Vittal V, Kolluri S, Mandal S. Decision tree-based preventive and corrective control applications for dynamic security enhancement in power systems. Power Syst, IEEE Trans 2010;25(3):1611–9.
[25] Esmaili Masoud, Hajnoroozi Ali Akbar, Shayanfar Heidar Ali. Risk evaluation of online special protection systems. Int J Electr Power Energy Syst 2012;41 (1):137–44.
[26] Kundur P. In: Balu NJ, Lauby MG, editors. Power system stability and control, vol. 7. New York: McGraw-hill; 1994.

[27] Atmaca Erkan. A rank correlation based coherency measure for power systems. In: ELECO'2001, 2nd international conference on electrical and electronics engineering.
[28] Chow JH, Galarza R, Accari P, Price WW. Inertial and slow coherency aggregation algorithms for power system dynamic model reduction. Power Syst, IEEE Trans 1995;10(2):680–5.
[29] Safavian SR, Landgrebe D. A survey of decision tree classifier methodology. IEEE Trans Syst, Man, Cybern 1990;21(3):660–74.
[30] Pai A. Energy function analysis for power system stability. Springer Science & Business Media; 2012.
[31] http://ec.europa.eu/eurostat/statistics-explained/index.php/Electricity_price_statistics.
[32] Aghamohammadi Mohammad Reza, Shahmohammadi Ali. Intentional islanding using a new algorithm based on ant search mechanism. Int J Electr Power Energy Syst 2012;35(1):138–47.